ARL-TR-9424 • MAR 2022

DEVCOM ARMY RESEARCH LABORATORY

Designing Steels to Mitigate Failure during Ballistic Deformation (Summary Technical Report, Oct 2018–Sept 2021)

by Krista R Limmer, Jeffrey T Lloyd, Daniel M Field, Daniel J Magagnosc, B Chad Hornbuckle, Timothy R Walter, Christopher S Meredith, John D Clayton, and Phillip A Jannotti

NOTICES

Disclaimers

The findings in this report are not to be construed as an official Department of the Army position unless so designated by other authorized documents.

Citation of manufacturer's or trade names does not constitute an official endorsement or approval of the use thereof.

Destroy this report when it is no longer needed. Do not return it to the originator.

ARL-TR-9424 ● MAR 2022

Designing Steels to Mitigate Failure during Ballistic Deformation (Summary Technical Report, Oct 2018–Sept 2021)

Krista R Limmer, Jeffrey T Lloyd, Daniel M Field, Daniel J Magagnosc, B Chad Hornbuckle, Timothy R Walter, Christopher S Meredith, John D Clayton, and Phillip A Jannotti
DEVCOM Army Research Laboratory

REPORT DOCUMENTATION PAGE

Form Approved
OMB No. 0704-0188

1. REPORT DATE *(DD-MM-YYYY)*	2. REPORT TYPE	3. DATES COVERED (From - To)
March 2022	Summary Technical Report	1 October 2018–30 September 2021

4. TITLE AND SUBTITLE
Designing Steels to Mitigate Failure during Ballistic Deformation (Summary Technical Report, Oct 2018–Sept 2021)

5a. CONTRACT NUMBER

5b. GRANT NUMBER

5c. PROGRAM ELEMENT NUMBER

6. AUTHOR(S)
Krista R Limmer, Jeffrey T Lloyd, Daniel M Field, Daniel J Magagnosc, B Chad Hornbuckle, Timothy R Walter, Christopher S Meredith, John D Clayton, and Phillip A Jannotti

5d. PROJECT NUMBER

5e. TASK NUMBER

5f. WORK UNIT NUMBER

7. PERFORMING ORGANIZATION NAME(S) AND ADDRESS(ES)
DEVCOM Army Research Laboratory
ATTN: FCDD-RLW-MF
Aberdeen Proving Ground, MD 21005

8. PERFORMING ORGANIZATION REPORT NUMBER
ARL-TR-9424

9. SPONSORING/MONITORING AGENCY NAME(S) AND ADDRESS(ES)

10. SPONSOR/MONITOR'S ACRONYM(S)

11. SPONSOR/MONITOR'S REPORT NUMBER(S)

12. DISTRIBUTION/AVAILABILITY STATEMENT
Approved for public release: distribution unlimited.

13. SUPPLEMENTARY NOTES
ORCID IDs: Krista R Limmer, 0000-0003-4775-5876; Daniel M Field, 0000-0002-8890-4391; Daniel J Magagnosc, 0000-0002-1418-9292; Christopher S Meredith, 0000-0003-1368-8003; John D Clayton, 0000-0003-4107-6282; Timothy R Walter, 0000-0002-1786-3668

14. ABSTRACT
This summary technical report presents an overview of the key research activities, major technical outcomes, and impact from the 3-year basic research program entitled “Designing Steels to Mitigate Failure during Ballistic Deformation.” This program was successful in developing institutional knowledge and a framework for the design of novel ultrahigh strength steels for enhanced ballistic performance using transformation-induced plasticity and twinning-induced plasticity. Engineering of the austenite volume fraction and stability through alloy design and controlled processing identified future pathways for production of enhanced performance armor steels. The advanced understanding of the phase transformation has potential applications beyond armor as well.

15. SUBJECT TERMS
STR, steel, armor, deformation mechanism, constitutive modeling, alloy design, mechanical testing, neutron diffraction, TRIP, TWIP

16. SECURITY CLASSIFICATION OF:			17. LIMITATION OF ABSTRACT	18. NUMBER OF PAGES	19a. NAME OF RESPONSIBLE PERSON
a. REPORT	b. ABSTRACT	c. THIS PAGE			Krista R Limmer
Unclassified	Unclassified	Unclassified	UU	40	19b. TELEPHONE NUMBER (Include area code) (410) 306-2039

Standard Form 298 (Rev. 8/98)
Prescribed by ANSI Std. Z39.18

Contents

List of Figures

List of Tables

Acknowledgments

From the US Army Combat Capabilities Development Command Army Research Laboratory, the authors would like to thank Jonathan Montgomery, Rich Becker, and Scott Schoenfeld for their mentorship throughout this program. Mechanical testing support for portions of the program were provided by Levi Johnson, James Paramore, Brady Butler, and Trevor Hastings. The authors would also like to thank Cyril Williams and Scott Turnage for the shock testing. The advanced in-situ characterization was made possible with assistance from Oak Ridge National Laboratory's (ORNL's) Matthew Frost and Ke An. Finally, the authors acknowledge the ORNL Spallation Neutron Source for beam time access.

Executive Summary

The topic of this 3-year, 6.1 basic research program was a paradigm shift from conventional automotive advanced high-strength steel (AHSS) alloy design—that is, the design of ultrahigh-strength steels that prevent severe shear localization rather than obtain global formability. Our hypothesis stated that mechanisms that dominate during homogeneous quasi-static and moderate-rate dynamic tests will not globally perform in ultrahigh-strength steels under ballistic loading conditions. To test this hypothesis we designed and evaluated steel microstructures that will activate mechanisms to locally short-circuit catastrophic failure during ballistic impact: twinning-induced plasticity (TWIP) to suppress the propagation of shear localization bands and transformation-induced plasticity (TRIP) to blunt fast-propagating crack tips. Shear localization was further investigated by the design of dispersion strengthening agents through the tailoring of morphology, distribution, and interface strength of secondary and tertiary phases.

Through the four phases of the program, key developments were made to understand and predict activation of deformation mechanisms during ballistic events. In Phase 1, austenitic steels with varying stacking fault energy (SFE) levels were designed, produced, tested, and characterized with ex-situ and in-situ methods. This large suite of data was used to parameterize continuum scale models that incorporate TWIP and TRIP behavior. These models were validated using Taylor rod impact testing. In Phase 2, dual-phase alloys were engineered to control the amount and stability of austenite and to push the alloys to armor-strength levels. The testing and characterization of these armor-strength alloys included additional methods to better understand the effect of TRIP and TWIP on localization and failure at high rates. Phase 3 designed and produced larger plate volumes to enable ballistic testing and incorporate carbides as a means of increasing strength and toughness without changing the austenite content and TRIP/TWIP ability of the alloys. Phase 4 explored use of the TRIP mechanism to disrupt shock waves. It was also the first work to demonstrate the feasibility of this method through experimental and computational means.

This program was greatly successful and made several key advancements in the steel processing–property–performance design space. We found that processing routes can be specifically engineered to tailor microstructures that give favorable dynamic mechanical properties. This methodology is based on key experimental, analytical, and computational accomplishments in this work that were used to develop a methodology to link intrinsic microstructural features such as composition of individual phases and microstructure feature size to quasi-static and dynamic mechanical response via intermediate quantities (e.g., SFE and driving

forces for phase transformation). Based on our understanding of the thermodynamic driving force for transformation, we found that under dynamic loading conditions TRIP and TWIP materials are in a race against temperature rise. During dynamic deformation the beneficial fracture properties are achieved when transformation is delayed until finite strains. Materials with too much of the initial transforming phase are unstable and will transform immediately, losing all potential for the transformation to interact with failure mechanisms that occur at later times (i.e., void and crack opening). In Phase 1 this was found by increasing the strength of an austenitic steel through prestraining to give enhanced high-rate performance, whereas, in Phase 2 heat treatment was used to affect phase stability and volume fraction that intrinsically increased strength and delayed phase transformation. Finally, the preliminary work on leveraging the compositionally controlled phase transformation has opened up a new field on controlling shock waves at US Army-relevant pressures.

1. Mission Description and Introduction

In this program, our goal was to understand the relationships required to design an engineered multiphase steel to take advantage of both high strength and a range of deformation mechanisms to prevent severe shear localization in armored materials. We hypothesized that for a multiphase steel with an engineered microstructure, specific deformation mechanisms to locally short-circuit catastrophic failure could be activated during ballistic impact. In particular, twinning-induced plasticity (TWIP) would be activated to suppress the propagation of shear localization bands. Transformation-induced plasticity (TRIP) would be activated to blunt fast-propagating crack tips. Shear localization would also be affected through the design of dispersion-strengthening agents (e.g., carbides). This design process included determining how the primary phases (α, α', γ) deform at various loading rates, how grain size and phase heterogeneity affect the dominant deformation mechanisms, and how shear localization can be strategically altered using precipitates.

2. Program Objectives

Our hypothesis is a paradigm shift from conventional automotive advanced high-strength steel (AHSS) alloy design—that is, the design of ultrahigh-strength steels that prevent severe shear localization rather than obtain global formability. We do not expect that mechanisms that dominate during homogeneous quasi-static and moderate-rate dynamic tests will globally perform in ultrahigh-strength steels under ballistic loading conditions. The objectives of this program are threefold:

1) Understand the mechanisms in ferrous alloys that enable resisting shear-dominated failure modes during ballistic impact through synchronous computational and experimental design of tailored deformation mechanisms under extreme loading rates.

2) Demonstrate, for a multiphase armor-strength steel, the mechanisms activated during a ballistic event that can be used to mitigate crack propagation.

3) Develop a framework by which future armor-steel alloys and processing can be designed.

To accomplish these objectives, we designed a microstructure that will activate mechanisms to locally short-circuit catastrophic failure during ballistic impact: TWIP will activate to suppress the propagation of shear localization bands and TRIP will activate to blunt fast-propagating crack tips. Shear localization will further be affected by the design of dispersion-strengthening agents through the

tailoring of morphology, distribution, and interface strength of secondary and tertiary phases.

Current State of the Art

Since the invention of TRIP steels in 1967,[1] the DOD has been at the forefront of determining what role metastable phase transformation can play in dynamic loading applications. Although these materials have desirable quasi-static properties (high toughness, very-high-strain hardening, reasonable ductility), the dynamic strength response is often *weaker*, which is the opposite of what occurs for almost all known metals.[2] The extreme temperature sensitivity of the TRIP mechanism means that adiabatic heating during dynamic deformation either retards or fully suppresses deformation-induced transformation, making the steels expensive with low-strength and moderate-strain hardening. Their deficiency in penetration[3,4] and blast loading[5,6] environments is well documented. On the other hand, recent work has demonstrated that by carefully controlling the stability of transforming phases, improvements in dynamic fracture and ballistic properties can be achieved.[7] Phase-stability engineering has mostly been empirical and confined to quasi-static settings; therefore, one of this work's key motivations is to better understand how phase stability evolves under dynamic loading environments and can be engineered during processing.

The novel concept of this work is the hypothesis that twinning and phase transformation can be exploited in high-strength steels to drastically increase their fracture toughness under dynamic-loading conditions without significantly reducing strength. These mechanisms have been capitalized on in the automotive industry to create moderate-to-high-strength, formable-sheet-steel components, although a direct translation to enhanced armor plates has not been realized. A fundamental understanding of how deformation mechanisms in each phase of multiphase steels respond to loading conditions that occur during penetration such as high-rate, high-temperature deformation is currently lacking and must be achieved through the course of the proposed research.

Several computational and experimental capabilities necessary for this program's success are unique to the US Army Combat Capabilities Development Command (DEVCOM) Army Research Laboratory's facilities and other recently developed national facilities and are enhanced during this program. Computationally, simulating large deformation, fracture, and failure requires significant resources as well as codes with mesh remapping algorithms such as ALE3D, to which DEVCOM Army Research Laboratory (ARL) researchers make significant contributions. Experimentally, the electron microscopy expertise of this team

allows us to rapidly analyze dominant deformation mechanisms in the specimens tested under high-rate, high-temperature conditions. Ballistic testing with advanced instrumentation is not only able to identify dominant failure modes during penetration, but also the order in which they occur. Although raw material (e.g., cast ingots) acquisition is contracted, DEVCOM ARL's processing facility with hot rolling plates and capability to perform heat treatments enables different processing routes to be explored. The initial state of the fabricated material is characterized using novel 2- and 3-D techniques. An atom probe is used to determine whether element clustering or segregation occurs near phase boundaries. The Oak Ridge National Laboratory (ORNL) Spallation Neutron Source (SNS) is used to quantify the stress state of the individual stages during heat treatment and partial deformation—to determine stability of phases as a function of temperature.

DEVCOM ARL has uniquely skilled and focused employees with access to institutional knowledge, particularly in the required area of ballistic mechanisms, including high-strength steel metallurgists, characterization and high-rate mechanical testing experts, and ballistics mechanisms application and modelling. Steels have not been optimized for ballistic performance (only incremental enhancements exist in the past decades); however, we now have the tools to do this and make significant advancements.

3. Research Efforts

3.1 Introduction

The primary objective of this work was to build a framework that correlates a material's microstructure (e.g., composition and heat treatment) with dominant deformation mechanisms over a range of loading conditions. This framework was built on the understanding and control of deformation mechanisms and demonstration of their activation during ballistic events. Models were developed at multiple length scales to represent, with high fidelity, the characteristics of the complex multiphase materials required for the mechanistic understanding. Microscale models were developed to inform process–structure–property relationships that feed into macroscale models developed for performance simulations.

Program execution was such that computational and experimental efforts were conducted synchronously across four general task areas: 1) alloy design and processing, 2) mechanical testing and ballistic evaluation, 3) characterization, and 4) continuum modeling. These task areas and their connectivity are schematically shown in Fig. 1 with representative images for each.

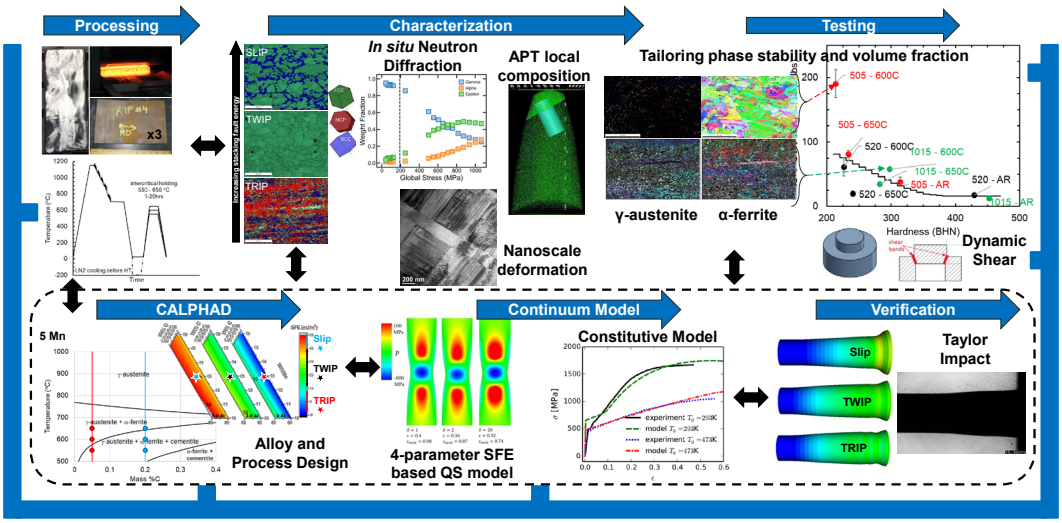

Fig. 1 Schematic representing concurrent design, experimental, and computational aspects; and the information flow between task areas*

An initial understanding of the dominant deformation mechanisms and their effect on properties (i.e., strength, strain hardening, and fracture toughness) was built using empirical observations of a range of carefully chosen single-phase and multiphase steels. This understanding was then quantified in a model that is able to predict the component-level deformation response of a multiphase steel subjected to high-speed penetration. The developed models needed to be robust and efficient enough to solve such engineering-scale problems, but must also be able to guide material design by containing either explicit treatment of heterogeneous microscale features, or have internal state variables that represent prominent features that arise from processing. This program was designed with a three-phase approach:

Phase 1. *Mechanism Activation Kinetics*: Determining the kinetics and activity of deformation mechanisms in three austenitic alloys with varying stacking fault energy (SFE).

Phase 2. *Fracture, Localization, and Failure*: Evaluation of multiphase steels, and an expansion of the characterization suite of tools including testing fracture, localization, and failure.

Phase 3. *Strength Optimization and Ballistics*: Optimization of strength in a multiphase steel with secondary strengthening subjected to ballistic loading.

* Inset figures are representative of significant task area outcomes and can be found throughout the report in more detail.

The COVID-19 pandemic (which began in the middle of the second year of the program) resulted in access and timing constraints; therefore, a limited approach to Phase 3 was undertaken and supplemented with the fourth phase:

Phase 4. *Shock Wave Manipulation*: Leverage the TRIP effect to disrupt shock waves in a compositionally controlled SFE gradient material.

Highlights of the significant actions and results for each program phase are summarized in the following sections. Readers are referred to the publications (Section 7) for further details throughout.

3.2 Phase 1: Mechanism Activation Kinetics

The objective of this phase was to determine the kinetics and activity of deformation mechanisms in three austenitic alloys with varying SFE to make a mechanical model that depends on composition, loading rate, and temperature—but has few enough parameters and is robust and fast enough to apply to ballistic loading applications. The three alloys used in this phase were designed using the calculation of phase diagrams (CALPHAD) method to be primarily austenitic and have a wide range of SFE. The alloys' SFE was controlled by varying carbon and aluminum contents, with the same amount of silicon, manganese, and chromium used in each alloy, with iron as the balance. The composition in weight percent (wt%) of each alloy is provided in Fig. 2. These three alloys are referred to using their predicted room temperature deformation mode (TRIP, TWIP, or slip) according to their predicted SFE as shown in Fig. 2. Ingots (50 lbs) were acquired and controlled and hot-rolled to a nominally 0.5-inch plate at DEVCOM ARL with subsequent heat treatment to stress-relieve the plates.

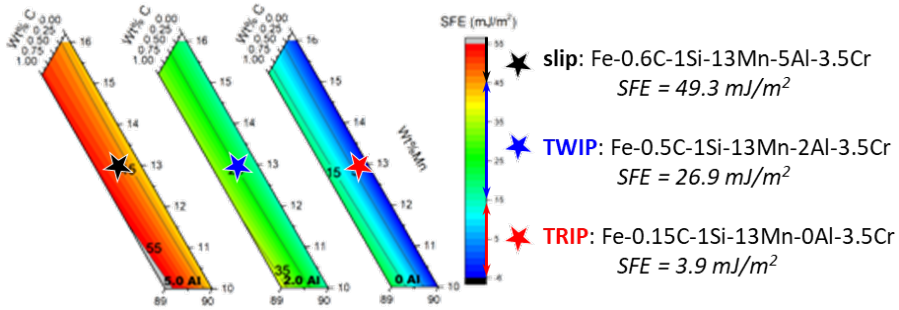

Fig. 2 Composition and calculated SFE of the TRIP, TWIP, and slip alloys used in Phase 1*

The starting microstructures of the three alloys shown in Fig. 3 demonstrate that a single-phase, face-centered cubic (fcc) austenitic structure was only observed for

* Compositions provided are in wt%.

the TWIP alloy. The slip alloy was composed of large austenite grains surrounded by fine body-centered cubic (bcc) ferrite grains. The TRIP alloy contained a large starting volume fraction of hexagonal close-packed (hcp) ε-martensite, which was expected as an intermediate phase during the $\gamma \rightarrow \alpha$ phase transformation. The phase volume fractions were also measured with X-ray diffraction to try a larger sample volume and they had similar results.

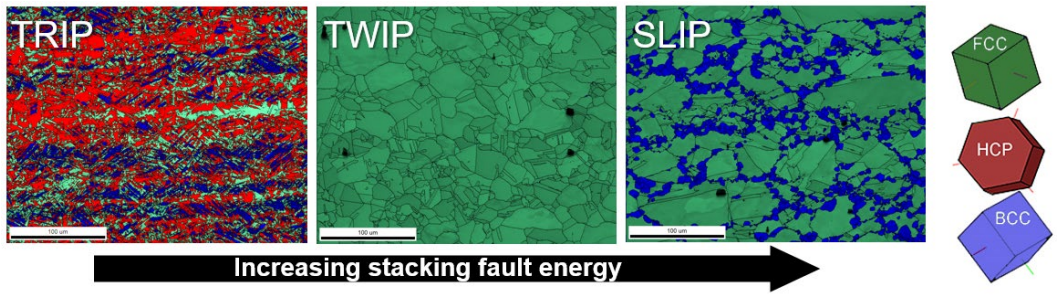

Fig. 3 Electron backscatter diffraction (EBSD)-orientation image mapping (OIM) images of the initial microstructure of the TRIP, TWIP, and slip alloys

Mechanical testing was performed on each alloy at a range of loading rates and temperatures in tension and compression. Quasi-static (0.001/s) and dynamic (~2500/s) testing were performed at room temperature and at 200 °C. Representative room temperature true-stress versus true-strain results for each alloy are shown in Fig. 4. Limited tension compression asymmetry was observed and the dynamic strength was higher than quasi-static rates as anticipated.

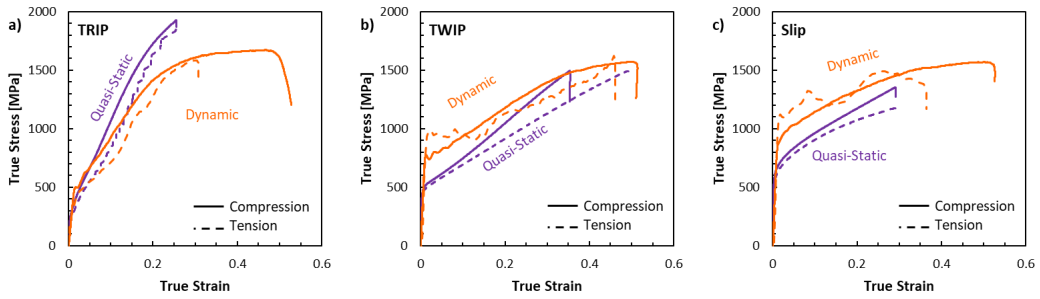

Fig. 4 Representative true-stress vs. true-strain curves for TRIP, TWIP, and slip alloys tested in tension and compression at quasi-static and dynamic rates at room temperature

High temperature (200 °C) mechanical testing was performed for quasi-static tension and compression as well as dynamic compression. Figure 5 shows representative true-stress versus true-strain curves for each alloy as a function of testing temperature.

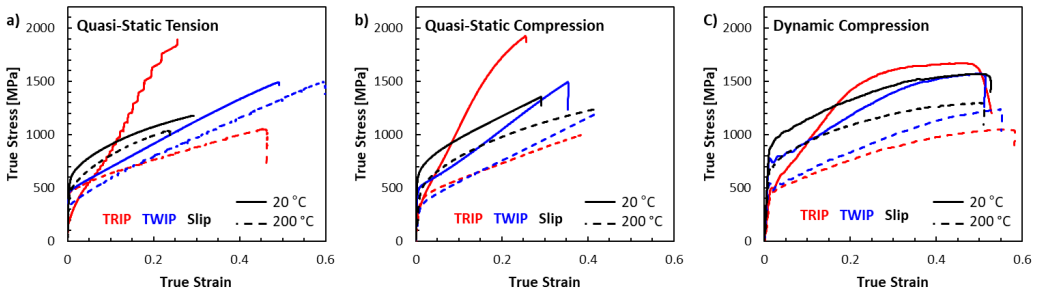

Fig. 5 Representative true-stress vs. true-strain curves at room temperature and 200 °C for loading in quasi-static tension and dynamic compression

A thermodynamically consistent, geometrically nonlinear constitutive model for steels has been formulated with comprehensive features thought to be unique among models of this class. Details are available in a published article.[8] Encompassed are nonlinear thermoelasticity relevant for high pressure/shock loading, viscoplasticity for slip and twinning across a wide range of temperatures and strain rates, ductile damage growth, and martensitic phase transformations affected by stress state, temperature, and loading rate. Volume changes associated with porosity and phase changes are included. The model has been demonstrated as capable of representing data on three different alloys with very different hardening behaviors and deformation mechanisms. Extrapolations of the model to conditions pertinent to the shock regime appear physically reasonable, though validations of strength predictions in this regime await experiments on these particular alloys. Model predictions for simultaneous simple shear with tension or compression suggest how different physical mechanisms in the three steels should affect their tendency for localization and dynamic failure.[8] These results suggest that the TWIP alloy would perform best for ballistic applications dominated by shear and compressive strain states (e.g., thick-target penetration), while the TRIP alloy would perform well in ballistic applications wherein tensile strain dominates (e.g., spall).

The continuum models for TWIP, TRIP, and slip steels more recently implemented in dynamic ALE3D simulations qualitatively capture different deformation patterns among these materials in Taylor impact (Fig. 6). Quantitative analysis is ongoing.

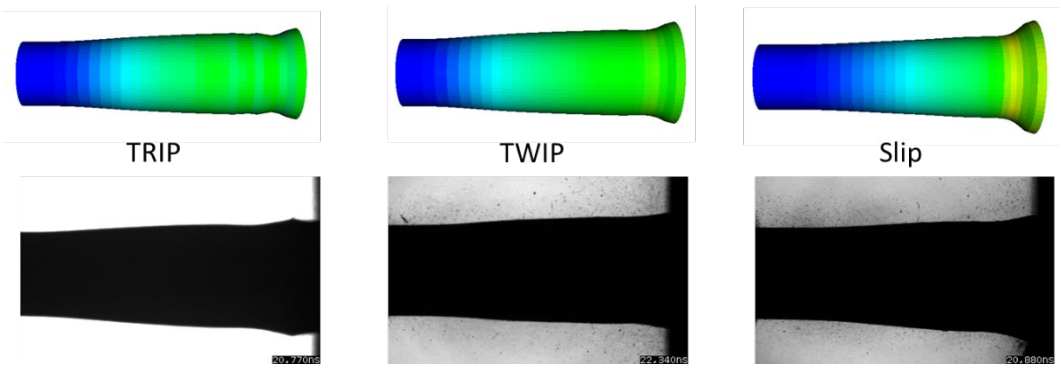

Fig. 6 Alloy-dependent model predicted deformation geometry and observed geometry during Taylor impact testing

A simple, robust strength model was also developed to predict hardening behavior in medium-manganese steels.[9] The model shown in Fig. 7 predicts rapid failure in TWIP and TRIP steels because of the rate of decrease in hardening rate. The model parameters are computed based on the SFE as a function of composition, grain size, and testing temperature. This model contains only four parameters making it significantly more lightweight than the full constitutive model. The key feature of this model is that the parameters are dependent on the SFE derived from the constitution and grain size.

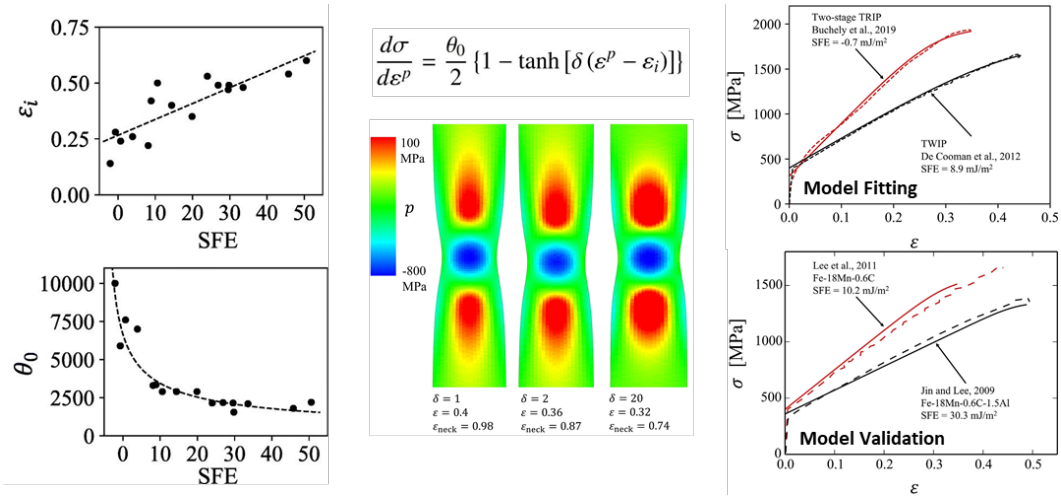

Fig. 7 Model relationship to predict hardening response $\left(\frac{d\sigma}{d\varepsilon^p}\right)$ with parameters (ϵ_i and θ_0) demonstrated as a function of SFE along with model fitting and validations

Beyond the constitutive model development, advanced understanding of deformation mechanism activation and load partitioning was pursued using the ORNL SNS. The three alloys were tested in tension from room temperature to 200 °C with neutron-diffraction data collected during tensile testing to enable in-situ phase analysis coupled with the mechanical response. The complexity of the

data enabled in-depth mechanistic understanding to be developed for each alloy as the following summarizes.

The slip alloy comprises a bimodal duplex microstructure consisting of coarse-grained γ-austenite with fine δ-ferrite grains decorating the γ-austenite boundaries as shown in Fig. 8. The coarse-grained high-SFE γ-austenite deformed by dislocation glide provides work hardening and ductility. Simultaneously, the fine-grained δ-ferrite produced an elevated yield strength by strengthening the steel via a composite-reinforcing mechanism. The SNS testing results enabled tracking specific diffraction peaks during loading to identify phases and further delineate the load-partitioning behavior during mechanical testing. As shown in Fig. 8d the austenite phase shows little change with increasing temperature while the δ-ferrite exhibits pronounced softening. Neutron diffraction reveals that the yield-strength reduction at elevated temperatures is caused by a reduction in the δ-ferrite strength. Additional details of the testing, characterization, and analysis have already been published.[10]

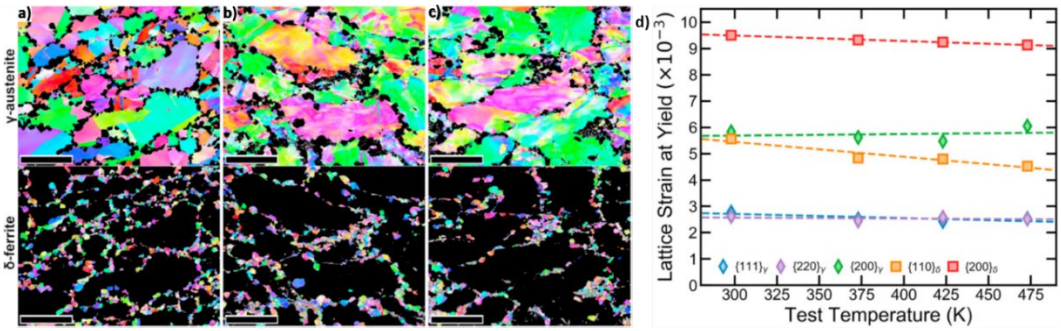

Fig. 8 Slip alloy EBSD orientation images with 100-μm scale bar partitioned into austenite and ferrite phase in the a) as-rolled, b) room temperature tensile test, and c) room temperature of 200 °C tensile-tested conditions. d) Neutron diffraction measured lattice strain at macroscopic yield for diffraction peaks as a function of test temperature with linear fits to guide the eye.

The TWIP alloy consisted of a fully austenitic structure and twinned during deformation as shown in Fig. 9. In-situ tensile loading at multiple temperatures enabled the calculation of the temperature and strain dependence of the effective SFE, which was compared with theoretical SFE calculations and ex-situ tensile tests. These comparisons revealed that the γ-austenite/ϵ-martensite interfacial energy plays a critical role in determining the boundary between TWIP and TRIP. The interfacial energy, which also exhibits temperature dependence, was found to be lower than the conventionally accepted range for medium-manganese steels deforming via twinning. Dynamic strain aging (DSA) was also found to impact the deformation response. DSA contributes to increasing the separation of partial dislocations, which in turn lowers the effective SFE and was observed as

fluctuations in the measured SFE when DSA was active. The additional extrinsic contributions to the SFE from DSA, which operates over a limited range of temperatures and strain rates, has not been accounted for previously. Additional details of the testing, characterization, and analysis are being published; see the publication list (Section 7) for status of this manuscript at the time of reporting.

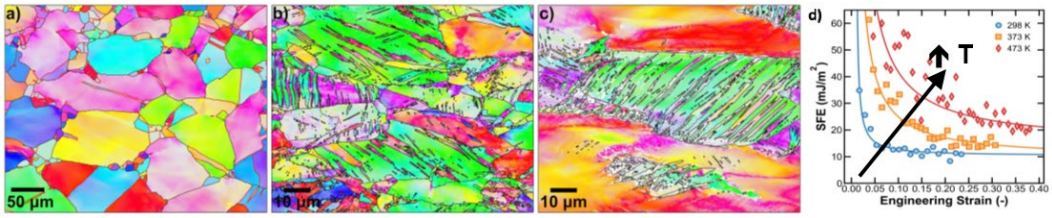

Fig. 9 EBSD orientation maps revealing the microstructure for the a) as-rolled, b) tested at 20 °C, and c) tested at 200 °C TWIP alloy. d) SFE determined for each increment of the in-situ tensile tests with empirical fits of the functional form 1/x are included to guide the eye.

The TRIP alloy was a triplex microstructure consisting of austenite, ε-martensite, and α-martensite as seen in Fig. 3. During deformation the austenite transforms (i.e., TRIPs) to ε-martensite and with additional deformation the ε-martensite further transforms to α-martensite. In-situ investigation of the deformation response at multiple temperatures was performed using neutron diffraction to isolate deformation and transformation of each phase during loading. Increasing temperature decreased the driving force for phase transformation while the propensity for twinning deformation increased. These results correlated well to the regular solution model used to design the Phase 1 steels. Further, the critical stress for twinning was higher than the critical stress for ε-martensite formation—leading to the TRIP steel producing an increase in strength as the temperature was raised. Ex-situ investigation of the steel showed that twinning became the dominant deformation mechanism when the temperature was greater than 150 °C and dislocation slip started to become apparent as the deformation temperature was raised to 200 °C as seen in Fig. 10. Further details of the testing, characterization, and analysis are being published; see the publication list (Section 7) for the status of this manuscript at the time of reporting.

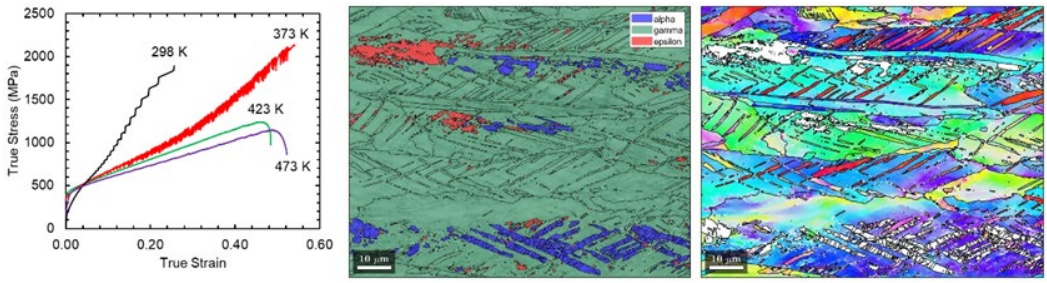

Fig. 10 a) Mechanical response of the TRIP alloy after testing at multiple temperatures (298–473 K), b) phase, and c) orientation image map of just the γ-austenite from the steel after tensile testing at 473 K

3.3 Phase 2: Fracture, Localization, and Failure

The objective of this phase was to evaluate intentionally multiphase high-strength steels and expand the characterization suite of tools to include fracture, localization, and failure. To achieve this objective a series of four steel alloys were designed with varying manganese and carbon levels to control austenite stability as shown in Fig. 11. The volume fraction and composition of the austenite was controlled by intercritical annealing. Because austenite is the phase that can TRIP or TWIP during a ballistic event, better understanding the role of its stability and volume fraction on the activation of these mechanisms is critical.

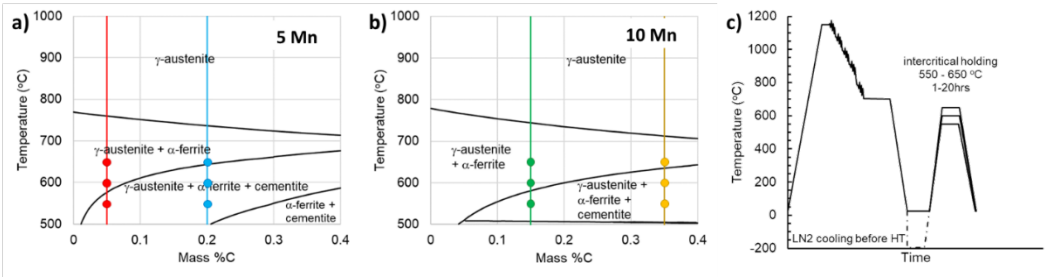

Fig. 11 Equilibrium phase diagrams for Phase 2 alloys with circles indicating intercritical annealing temperatures of a) 5 wt% Mn-alloys 505 (red) and 520 (blue), and b) 10 wt% Mn-alloys 1015 (green) and 1035 (yellow). c) Processing schematic includes hot-rolling, quench temperatures, and intercritical annealing.

Carbon diffusion during intercritical annealing in the γ + α phase field changes the austenite carbon saturation level as a function of time and temperature, which affects the volume fraction and stability. The volume fraction of austenite is readily measured using X-ray powder diffraction or EBSD and increases with annealing time and temperature as shown in Fig. 12 for the 520 alloy (Fe – 0.20 C – 5 Mn – 0.2 Si – 0.2 Al wt%).

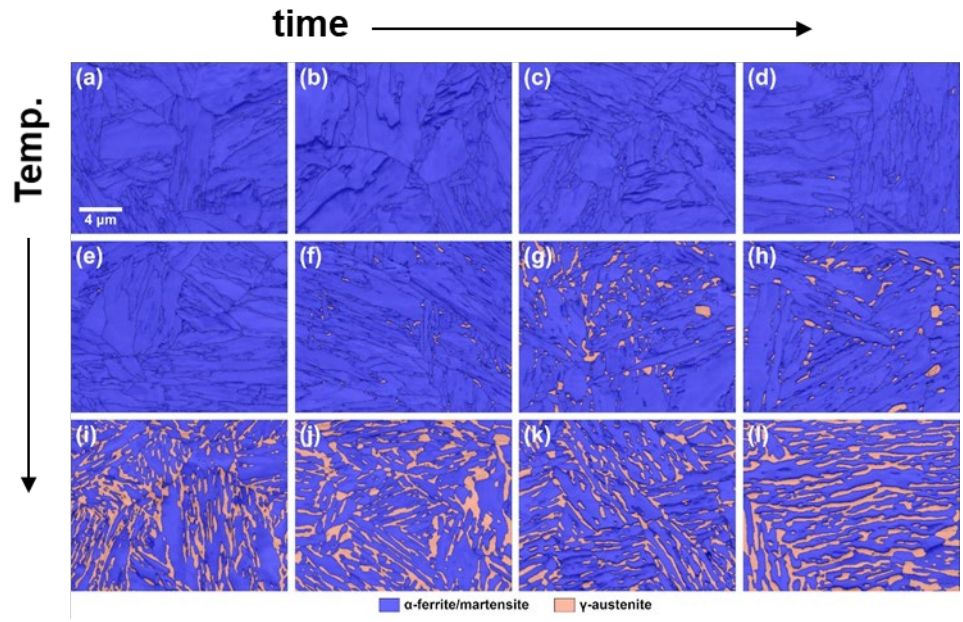

Fig. 12 Intercritical annealing effect on microstructure of 520 alloy indicating the increase in volume fraction with increasing annealing temperature and time

As the austenite volume fraction increases, the austenite stability is expected to decrease due to broader distribution of carbon required by mass balance. Given a finite amount of carbon, when it is distributed across a larger total volume, each volumetric unit contains a smaller amount and affects the local stability. This local composition was quantified using atom probe tomography as shown in Fig. 13. Intercritical annealing for 20 h at a higher temperature increased the volume fraction of austenite, but also reduced the carbon and manganese concentration of the austenite. This decrease in austenite carbon and manganese translates to a reduction in the thermal and mechanical stability of the austenite as measured according to the martensite start temperature, which is a function of the driving force for transformation. The driving force for transformation was decreased due to the lower heat treatment temperature; therefore, the alloy exhibited increased Charpy toughness at lower temperatures from the activation of twinning as opposed to phase change.

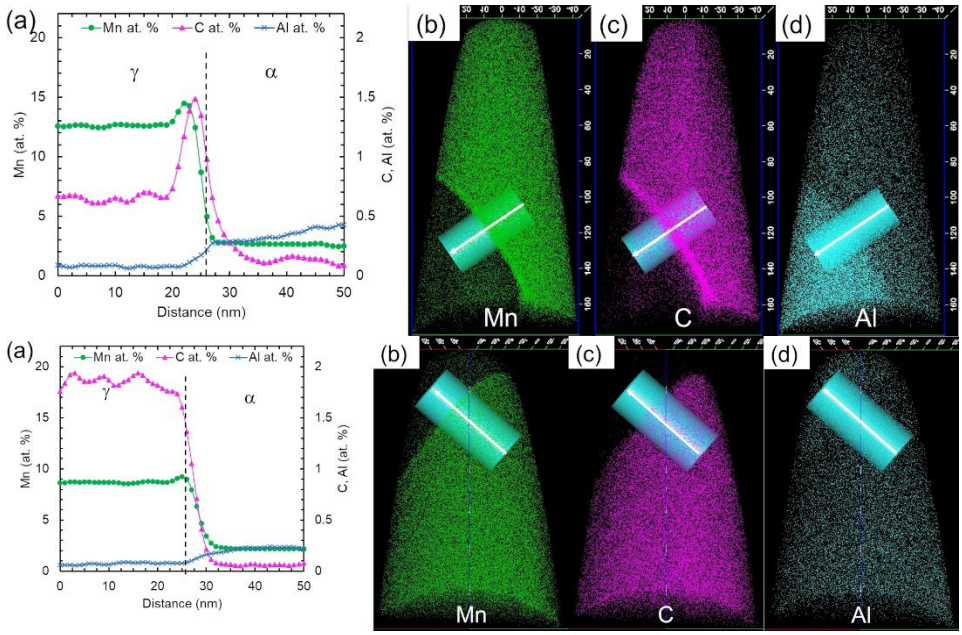

Fig. 13 Composition profile at the γ-α interface in alloy 520 after intercritical annealing for 20 h at 600 °C (top) and 650 °C (bottom)

Mechanical testing was performed to assess the deformation response of the alloys. Quasi-static (0.001 s^{-1}) tension and compression along with dynamic (~2500 s^{-1}) compression were evaluated as shown in Fig. 14. For each of the alloys, increasing the intercritical annealing (ICA) temperature produced an increased austenite volume fraction that results in a lower yield strength, increased work hardening, and total elongation in tension testing. No significant tension–compression asymmetry was noted and the dynamic yield strength was higher as expected. A comparison of the tensile toughness, defined as the area under the stress–strain curve, indicates that alloy 1015 with a 650 °C ICA treatment has both the highest strength and most ductility. Therefore, it is the best engineering alloy. Because this is a measure based on quasi-static tensile loading, it is not surprising that this measure does not correlate with ballistic performance. Further analysis of the load partitioning and activation of deformation mechanisms is ongoing following neutron-diffraction experimentation at ORNL SNS.

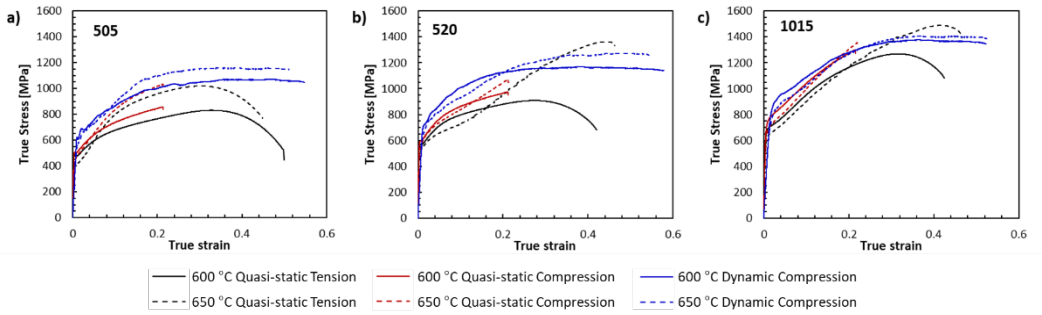

Fig. 14 Representative mechanical response of the Phase 2 alloys: a) 505, b) 520, and c) 1015 in two different heat-treated conditions (600 °C and 650 °C)

In addition to the tension and compression testing, hardness and Charpy v-notch (CVN) impact testing were also performed and compared against the requirements of a Class 1 rolled homogeneous armor steel.* More than half of the alloy-treatment combinations fall above the minimum acceptance line shown in Fig. 15. In all cases the formation of austenite during the ICA treatment reduced the hardness from the as-rolled condition with similar hardness levels attained for both ICA treatments in agreement with the uniaxial strength results above. In all cases the 600 °C ICA treatment, which formed less (but more stable) austenite, produced a higher impact energy.

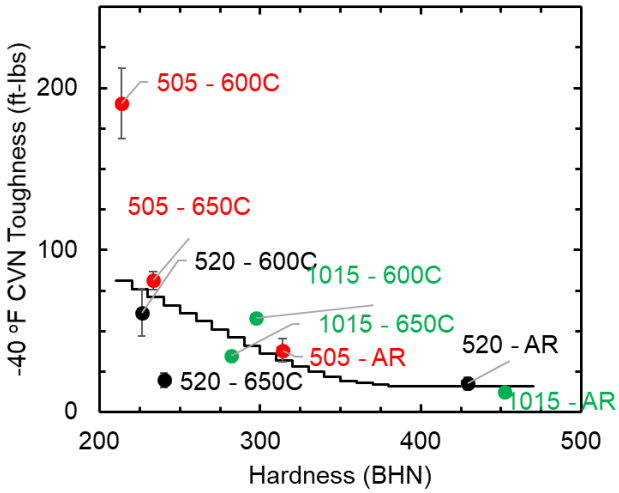

Fig. 15 CVN impact energy as a function of hardness for the three Phase 2 alloys fully investigated indicating the effect of ICA treatment temperature or the as-rolled condition on alloy performance†

Taylor rod impact testing was also performed for validation of the constitutive model. The quantitative evaluation of these results is ongoing. The qualitative

* As specified by MIL-DTL-12560K.
† MIL-DTL-12560K minimum acceptance criteria is shown as the solid black line for reference.

results are in agreement with the mechanical testing results; the degree of deformation observed is shown in Fig. 16. Samples with increasing strength and decreasing CVN toughness were observed to have brittle failure at lower velocities than the tougher materials.

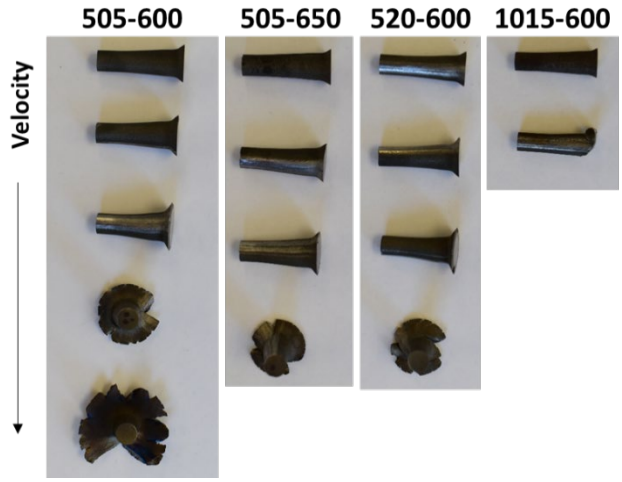

Fig. 16 Plastic deformation of Taylor rod impact cylinders for four representative alloy-treatment combinations as a function of velocity*

This phase demonstrated that tailoring the austenite volume and stability significantly affects the properties and performance of wrought steel. Alloy design for enhanced ballistic performance will require further optimization of phase stability—not just the easy-to-measure volume fraction.

3.4 Phase 3: Strength Optimization and Ballistics

The objective of Phase 3 was to optimize the strength in a multiphase steel with secondary strengthening and to evaluate the performance under ballistic loading. As seen in Phase 2, the austenite stability can be controlled to provide better toughness for a given hardness. Carbides are another means to increase strength, although the type and volume fraction of these engineered carbides can also play a significant role in the toughness and performance of the steel alloy. To achieve the objectives of this program phase, six alloys were designed as shown in Table 1. These alloys are based on the Phase 2 alloys, although the carbon content of alloy 520 was decreased to produce alloy 515. Because molybdenum carbides are generally expected to be high performing due to their coherency in the steel matrix, molybdenum additions of 0.5 wt% were added to a second heat of each of the three base alloys to complete the set.

* Samples in the same row are at the same nominal velocity. Only velocities without brittle failure are shown.

Table 1 Target compositions of Phase 3 alloys provided in wt%

Alloy	C	Mn	Si	Al	Mo
505	0.05	5.0	0.2	0.2	0.0
505M	0.05	5.0	0.2	0.2	0.5
515	0.15	5.0	0.2	0.2	0.0
515M	0.15	5.0	0.2	0.2	0.5
1015	0.15	10.0	0.2	0.2	0.0
1015M	0.15	10.0	0.2	0.2	0.5

After "hot-rolling" to plate, the alloys were again treated with an ICA step at 600 or 650 °C to partition carbon and affect austenite stability and volume fraction. Molybdenum had no significant effect on the volume fraction of austenite after ICA, although it did refine the austenite grain size. The molybdenum-bearing alloys were also subjected to an additional tempering step at 204 or 530 °C to precipitate the molybdenum-carbides. Two conditions of each alloy were selected for detailed evaluation including quasi-static tensile, CVN, and ballistic performance.

Quasi-static tensile testing results shown in Fig. 17 indicate that both the yield and ultimate strengths are higher for molybdenum-bearing alloys. The tensile ductility also generally decreases.

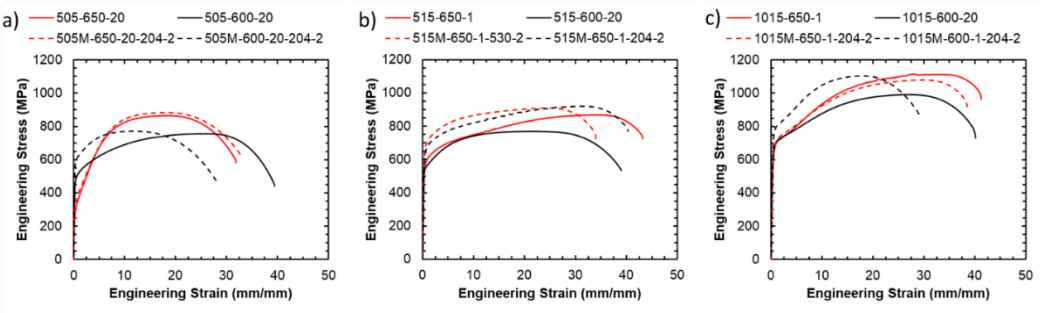

Fig. 17 Engineering stress–strain response for quasi-static tensile testing of Phase 3 alloys: a) 505 and 505M, b) 515 and 515M, and c) 1015 and 1015M*

Testing results compared to MIL-DTL-12560K requirements are shown in Fig. 18. The hardness–toughness relationship is enhanced by the molybdenum additions, with molybdenum-bearing alloys having increased hardness and/or toughness compared to their base alloy. Ballistic testing was performed using an armor piercing (AP) projectile and a fragment simulating projectile (FSP). The FSP performance decreased with increasing austenite volume fraction. The AP performance has historically been correlated with hardness. The results here follow that general trend; AP performance grew with increasing hardness or yield strength, although different interpretations of mechanisms can be drawn from these two

* Base alloys are shown with solid lines and molybdenum-added alloys are shown with dashed lines. Color is used to group comparable ICA treatments in each subfigure for clarity.

measures of strength. Full details on the ballistic testing, results, and analysis are being compiled in a limited distribution report.

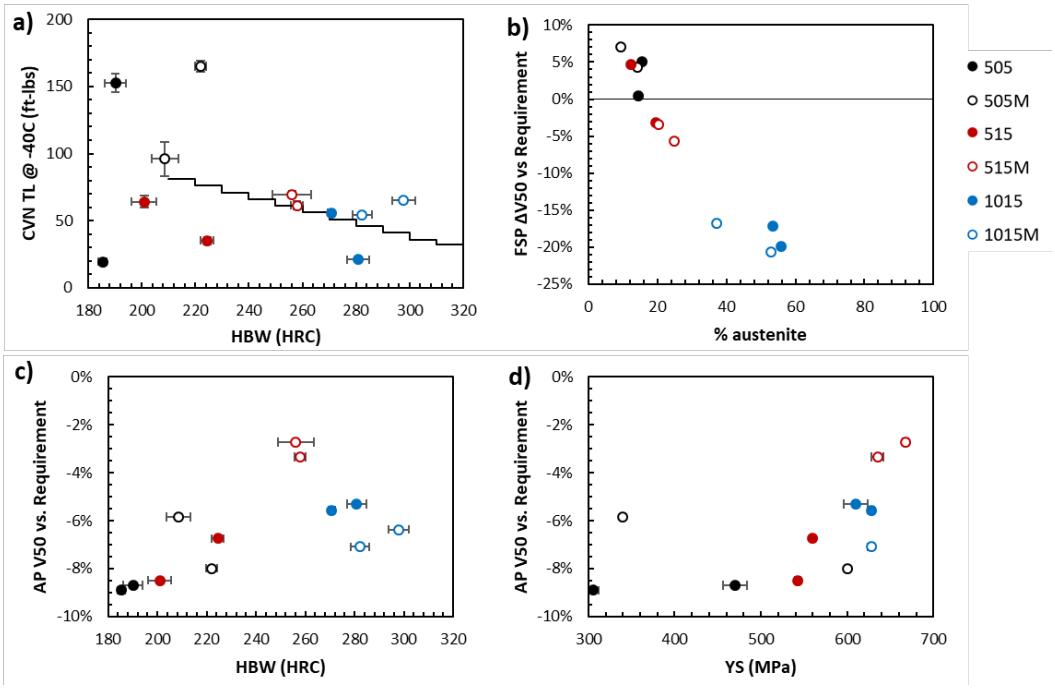

Fig. 18 Performance of Phase 3 alloys compared to MIL-DTL-12560K minimum requirements: a) CVN as a function of hardness, b) FSP performance vs. volume percent austenite, and AP performance as a function of c) hardness and d) yield strength

These large-scale testing results indicate that although increasing austenite volume fraction increases tensile toughness, the ballistic performance of these dual-phase steels does not continuously increase with tensile toughness. Rather, there is some maximum austenite volume fraction and other factors that must be considered during alloy design to meet specific performance metrics.

3.5 Phase 4: Shock Wave Manipulation

The objective of Phase 4 was to evaluate the volume contraction potential during the $\alpha \rightarrow \varepsilon$ phase transformation to disrupt shock waves. Existing solutions for disrupting shock waves employ low-density materials and mesostructures that occupy significant space, are difficult to fabricate, and are often destroyed after loading. Adding manganese to pure iron reduces the pressure of the transformation and the response time of this transformation is on the order of tens of nanoseconds, which is amenable to interacting with a shock wave. The $\alpha \rightarrow \varepsilon$ phase transformation is also reversible, which increases the probability of absorbing multiple shocks. A combination of experimental processing, testing, and

constitutive modeling were used to better understand the ability of this phase transformation to manipulate shock waves.

In addition to evaluating a single manganese alloying level, a gradient structure was created with roll bonding. The roll-bonded mesostructure consisted of three Fe-*x*Mn layers, where x = 4, 7, and 11 wt% Mn, which is shown schematically in Fig. 19 along with the interface microstructure.

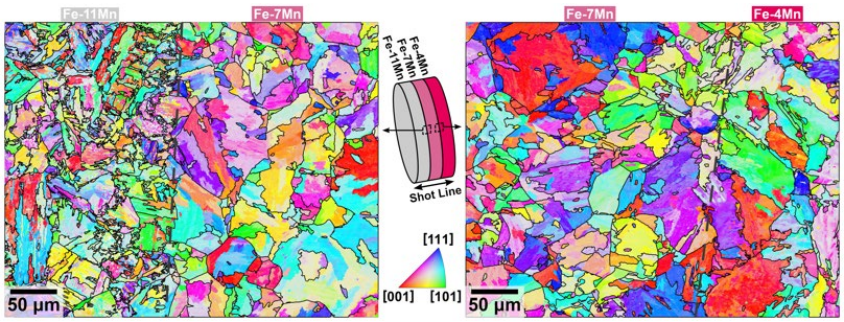

Fig. 19 Gradient structure (left) and microstructure (right) at interfaces

Plate-impact testing was performed on different layups for the individual alloys and for impact from low-to-high manganese content and high-to-low manganese content. The testing schematic and representative experimental and simulated velocities as a function of time are shown in Fig. 20. The simulated and measured velocities show effective shock disruption. Additionally, the recovered specimens reverted back to original phase, showing reversibility.

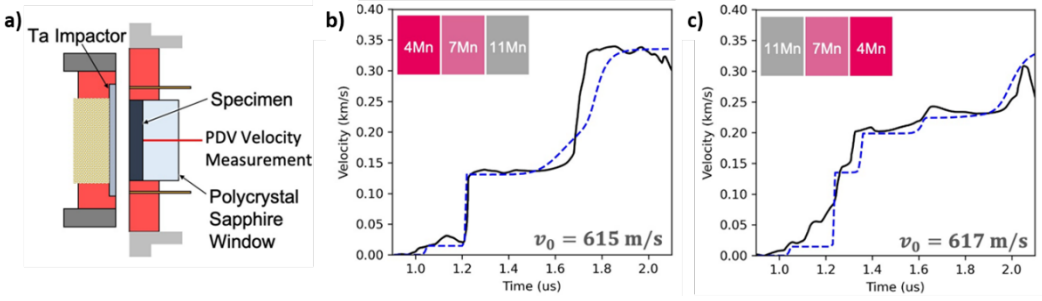

Fig. 20 Plate impact testing a) schematic of test setup and resulting velocity as a function of time for layup from b) low-to-high manganese content and c) high-to-low manganese content[*]

Continuum models successfully captured the most salient features of the problem and can be used for design in the future. Further 2-D simulations validated against planar experiments predicted geometries that can be used to effectively focus or dissipate shocks. This is the first work to demonstrate shock manipulation via alloying of phase-transforming metamaterials. Additional details are available in

[*] Black solid lines represent experimentally measured values and blue dashed lines represent continuum simulations.

Manipulating Shock Waves with Metallurgy by JT Lloyd et al.; see the publication list (Section 7).

4. Recommendations

- This project studied temperature sensitivity and thermodynamic stability of phases, which is key to enabling superior behavior of TRIP/TWIP steels under dynamic loading environments. However, other physical phenomena can also alter phase stability—such as external magnetic fields. Future work can explore the coupling between magnetic fields and phase stability, and whether magnetic fields can be used to extend the effective temperature range (and therefore dynamic strain level) that TRIP/TWIP can be active under.
- Preliminary work on utilizing composition gradients has proven that shocks can be manipulated and disrupted by composition alone. No optimization or specific application was identified for this work—mostly because the existing phase transformation model used in that work[11] is not particularly robust or generalizable to noniron materials. Making a more robust and generalizable phase transformation model with improved kinetics will be key to extending this basic research concept to specific applications of interest.
- The TRIP/TWIP steels used in this work were primarily low-to-intermediate strength due to the lack of intentional carbide precipitation and formation for simplicity. To achieve higher strengths we must extend our current framework and computational models to include carbide designs for maximum dynamic mechanical response.
- During this work the in-situ diffraction experiments and expertise we developed were extremely valuable for understanding material evolution during deformation. We propose to continue and expand on this capability, particularly at the ORNL SNS for other types of steels, metals, and ceramics.
- Advanced characterization methods closer to ballistic-impact conditions (i.e., Taylor impact experiments) were used to verify constitutive model parameters but did not influence model parameters. Emerging inverse methodologies have proposed to use experiments like these to refine model parameters in an automated fashion. We find that this approach is likely useful but was not pursued due to time constraints within the program.

Coupled dynamic in-situ measurements with inverse methods can provide a robust framework to evaluate material parameters.

- Prestrain effect on dynamic properties was demonstrated successfully, but no specific application was selected where final components could be fabricated from prestrained materials. To demonstrate the utility of this approach, ballistic impact experiments should be performed on the prestrained specimens in addition to other structural-level tests (i.e., can-crushing experiments in the automotive industry).
- Much of the work included in this report has been briefed to other DOD agencies during the DOD Steel Summit. We propose to continue this research and expand collaborations with other DOD agencies both in steel and in new phase-transforming materials.

5. Army Impact

- A framework to design, develop, manufacture, process, test, and evaluate next-generation steels for high-rate loading applications
- A fundamental understanding of whether volume change during phase transformation can be exploited to manipulate strain localization (broad implications for lethality and protection applications)
- The ability to isolate criticality under complex loading states in multiphase alloys; establish connections between microscale heterogeneity and macroscale behavior
- Processing routes to achieve targeted microstructure and performance in armor plates

6. Findings and Conclusion

Based on this work, processing routes can be specifically engineered to tailor microstructures that give favorable dynamic mechanical properties. This methodology is based on key experimental, analytical, and computational accomplishments that were used to develop a methodology to link intrinsic microstructural features such as composition of individual phases and microstructure feature size to quasi-static and dynamic mechanical response via intermediate quantities (i.e., SFE and driving forces for phase transformation [$\Delta G^{\alpha \rightarrow \epsilon}$ and $\Delta G^{\epsilon \rightarrow \gamma}$]).

Based on our understanding of the thermodynamic driving force for transformation, we found that under dynamic-loading conditions TRIP and TWIP materials are in a race against temperature rise. If the temperature rises sufficiently during adiabatic deformation, the SFE increases and the TRIP mechanism transitions to the TWIP mechanism and the TWIP mechanism transitions to slip. Because of their low strength, TRIP and TWIP steels that deform by dislocation glide are inherently inferior to conventional armor steels. To achieve very-high-strength TRIP/TWIP steels we quasi-statically prestrained the materials prior to dynamic deformation. Because there is little rate sensitivity on the initial strength response, the desired strength is determined by the quasi-static flow stress at a given strain level. In an example demonstration, we produced a TRIP steel that has an initial dynamic flow strength exceeding 1500 MPa with excellent strain hardenability. We did this by quasi-statically prestraining the material 10% to a flow stress of 1500 MPa (Meredith et al., forthcoming). This contrasts with the as-fabricated TRIP steel that had an initial flow strength of 500 MPa, which is much softer than is required for armor steels. A key next step will be to identify industrial and military processing routes that can be used to impart prestrain into these TRIP and TWIP steels.

Enabled by tracking deformation and phase-volume fraction via advanced in-situ diffraction experiments and compositional gradients across phases using ex-situ local electron atom probe experiments, TRIP materials with a greater amount of transforming phase (in most cases γ-austenite) often perform much worse dynamically than those with less of the transformation phase. This is because the elements that stabilize the phase are dispersed over a greater volume fraction. At the outset of this work, this finding was seemingly counterintuitive. During dynamic deformation, beneficial fracture properties are achieved when transformation is delayed until finite strains. Materials with too much of the initial transforming phase are unstable and will transform immediately, losing all potential for the transformation to interact with failure mechanisms that occur at later times (i.e., void and crack opening). This is most clearly demonstrated in Figure 19b, where materials with less austenite perform much better against blunt projectiles than materials with more austenite. This has been discussed thoroughly in *Phase Evolution in a TRIP Steel Dependent on Temperature and Strain Rate* by Field et al. (forthcoming) and agrees with the ballistic work performed by Zhang,[7] which states that small initial volume fractions of austenite (<20%) can yield significant improvements in ballistic performance against blunt projectiles.

At the outset of this program, we solely sought to use the dilatant volume expansion during $\gamma \rightarrow \alpha'$ and $\epsilon \rightarrow \alpha$ phase transformation to reduce the driving force for crack growth and void expansion in the presence of intense zones of localized deformation. However, once we understood and quantified how to engineer

materials to undergo phase transformations and their associated volumetric deformation under various loading states, we sought to understand whether the dilatant volume contraction during $\gamma \rightarrow \epsilon$ and $\alpha \rightarrow \epsilon$ phase transformation could be used in a beneficial manner. This led to our work that demonstrated how shock waves, which put the material under very high pressures, can be disrupted and manipulated by layering materials with difference-transformation pressures $P_0^{\alpha \rightarrow \epsilon}$, which are controlled by composition. We used planar shock-wave experiments and finite-element simulations to demonstrate for the first time how shock waves can be manipulated in Fe-*x*Mn layered structures that were roll-bonded, leading to a nearly 100-fold increase in shock rise times over monolithic materials. This finding has likely generated a whole new field that can be used to understand how composition, and not density, can be used to control shock waves at pressures relevant to DOD applications (up to 40 GPa).

7. Publications and Presentations

7.1 Publications

1. Lloyd JT, Field DM, Limmer KR. A four parameter hardening model for TWIP and TRIP steels. Mater Des. 2020;194:108878.

2. Clayton JD, Lloyd JT. A dynamic finite-deformation constitutive model for steels undergoing slip, twinning, and phase changes. J Dyn Behav Mater. 2021;7:217–247.

3. Magagnosc DJ, Field DM, Meredith CS, Walter T R, Limmer KR, Lloyd JT. Superior strength and ductility in a low density duplex steel studied by in situ neutron diffraction. Mater Sci Engineering: A. 2021;799:140252.

4. Magagnosc DJ, Field DM, Meredith CS, An K, TR, Limmer KR, Lloyd JT. Temperature and stress dependent twinning behavior in a medium-Mn TWIP steel. Acta Materialia. 2022.

Forthcoming Publications

5. Field DM, Hornbuckle BC, Magagnosc DJ, Lloyd JT, Limmer KR. Tailoring strength and toughness of a medium Mn steel. Metallurgical and Materials Transactions A (under review).

6. Lloyd JT, Magagnosc DJ, Clayton JD, Limmer KR, Turnage SA, Williams CL, Field DM. Manipulating shock waves with metallurgy. Acta Materialia (under review).

7. Limmer KR, Field DM, Magagnosc DJ, Walter TR, Meredith CS, Hornbuckle BC, Jannotti PA, Becker RC, Clayton JD, Lloyd JT. Designing steels: stacking fault energy effects in austenitic steels. DEVCOM Army Research Laboratory (US); (forthcoming).

8. Lloyd JT, Meredith CM et al. Improved dynamic strength of TRIP steel via pre-straining (forthcoming).

9. Field DM, Magagnosc DJ et al. Phase evolution in a TRIP steel dependent on temperature and strain rate (forthcoming).

10. Field DM, Limmer KR. Designing steels: development and evaluation of medium-Mn steels as wrought armor. DEVCOM Army Research Laboratory (US); (forthcoming).

7.2 Presentations

11. Field DM, Magagnosc DJ, Lloyd JT, Limmer KR. Ballistic behavior of medium-Mn steel: understanding composition and heat-treatment effects. Proceedings of the 2021 Department of Defense Steels Research Summit, virtual meeting; 2021 8–9 Nov.

12. Limmer KR, Field DM, Magagnosc DJ, Walter TR, Meredith CS, Lloyd JT. Stacking fault energy dependent deformation mechanisms in medium-Mn steels. Proceedings of the TMS 2022 Annual Meeting and Exhibition; 2022 2 Feb–3 Mar.

Planned Presentations

13. Magagnosc DJ, Limmer KR, Lloyd JT, Field DM. In situ neutron diffraction observations of steel deformation mechanisms. 2022 MACH Conference; 2022 6–8 Apr.

14. Meredith CS, Field DM, Magagnosc DJ, Walter TR, Lloyd JT, Limmer KR. Mechanical behavior and microstructural evolution of TRIP, TWIP, and slip multi-phase steels. 2022 SEM Annual Conference and Exposition on Experimental and Applied Mechanics; 2022 13–16 June.

8. References

1. Zackay VF, Parker ER, Fahr D, Busch R. The enhancement of ductility in high-strength steels. ASM Trans Quart. 1967;60(2):252–259.
2. Azrin M, Olson GB, Gagne RA. Inhomogeneous deformation and strain rate effects in high strength TRIP steels. Watertown, MA; 1973.
3. Weinstein D. Design mechanical properties for TRIP steel. 1969. Report No.: SRI Project 7722.
4. Kecskes LJ, Chen X, Li J, Vincent H, Wei Q, Jones TL. Evaluation of a belt-cast austenitic steel alloy from Salzgitter Mannesmann Forschung: Effect of hardness on the ballistic resistance against two 0.30-cal. projectile types. 2017.
5. McDonald B, Bornstein H, Langdon GS, Curry R, Daliri A, Orifici AC. Experimental response of high strength steels to localised blast loading. Inter J Impact Engineering. 2018;115:106–119.
6. McDonald B, Bornstein H, Ameri A, Daliri A, Orifici AC. Plasticity and ductile fracture behaviour of four armour steels. Inter J Solids and Structures. 2019;176:135–149.
7. Zhang XJ. Microhardness characterisation in developing high strength, high toughness and superior ballistic resistance low carbon Ni steel. Mater Science Technology (United Kingdom). 2012;28(7):818–822. doi:10.1179/1743284712Y.0000000015
8. Clayton JD, Lloyd JT. A dynamic finite-deformation constitutive model for steels undergoing slip, twinning, and phase changes. J Dyn Behavior of Mater. 2021:1–31.
9. Lloyd JT, Field DM, Limmer KR. A four parameter hardening model for TWIP and TRIP steels. Mater Design. 2020;194:108878.
10. Magagnosc DJ, Field DM, Meredith CS, Walter TR, Limmer KR, Lloyd JT. Superior strength and ductility in a low density duplex steel studied by in situ neutron diffraction. Mater Sci Engineering: A. 2021;799:140252.
11. Boettger JC, Wallace DC. Metastability and dynamics of the shock-induced phase transition in iron. Phys Rev B. 1997;55(5):2840.

List of Symbols, Abbreviations, and Acronyms

α	bcc phase, ferrite, or martensite
γ	fcc phase, austenite
ε	hcp phase, martensite
2-/3-D	two-/three-dimensional
Al	aluminum
AHSS	advanced high-strength steel
AP	armor piercing
ARL	Army Research Laboratory
bcc	body-centered cubic
C	carbon
CALPHAD	calculation of phase diagrams
CVN	Charpy v-notch
DEVCOM	US Army Combat Capabilities Development Command
DOD	Department of Defense
DSA	dynamic strain aging
EBSD	electron backscatter diffraction
fcc	face-centered cubic
Fe	iron
FSP	fragment simulating projectile
hcp	hexagonal close-packed
ICA	intercritical annealing
Mn	manganese
Mo	molybdenum
OIM	orientation image mapping
ORNL	Oak Ridge National Laboratory
SFE	stacking fault energy
Si	silicon
SNS	Spallation Neutron Source

TRIP	transformation-induced plasticity
TWIP	twinning-induced plasticity
wt%	weight percent

1 (PDF) DEFENSE TECHNICAL INFORMATION CTR DTIC OCA

1 (PDF) DEVCOM ARL
FCDD RLD DCI
TECH LIB

1 (PDF) DA HQ
DASA(R&T)

9 (PDF) USARMY AFC
L BROUSSEAU
R THYAGARAJAN
A LINZ
K WADE
S BRADY
J REGO
T KELLY
E JOSEPH
B SESSLER

2 (PDF) DEVCOM HQ
FCDD ST
C SAMMS
M HUBBARD

90 (PDF) DEVCOM ARL
FCDD RLC
C BEDELL
B SADLER
T PHAM
B PIEKARSKI
H EVERITT
FCDD RLC CA
L KAPLAN
FCDD RLC ES
G VIDEEN
S HILL
Y PAN
FCDD RLC I
B MACCALL
FCDD RLC N
BM RIVERA
A SWAMI
FCDD RLD
P BAKER
A KOTT
S SILTON
FCDD RLD D
T ROSENBERGER
FCDD RLD E
KS FOSTER
FCDD RLD F
K KAPPRA
FCDD RLD FR
M TSCHOPP
FCDD RLD SM
L BLUM
FCDD RLH
J CHEN
PJ FRANASZCZUK
C LANE
K MCDOWELL
FCDD RLH B
JJ SUMNER
FCDD RLH F
JR GASTON
FCDD RLH T
D STRATIS-CULLUM
FCDD RLL
T KINES
FCDD RLL D
J S ADAMS
FCDD RLL DP
J MCCLURE
FCDD RLR
B HALPERN
S LEE
D STEPP
FCDD RLR E
RA MANTZ
C VARANASI
FCDD RLR EL
JX QIU
MD ULRICH
FCDD RLR EN
RA ANTHENIEN JR
FCDD RLR IC
MA FIELDS
SP IYER
FCDD RLR IM
JD MYERS
FCDD RLR IN
XN WANG
FCDD RLR
P REYNOLDS
FCDD RLR P
LL TROYER
FCDD RLR PC
D POREE
FCDD RLR PL
MK STRAND
FCDD RLS
J ALEXANDER
M GOVONI
M WRABACK
FCDD RLS C
M REED
FCDD RLS CC
S BEDAIR

FCDD RLS CE
TR JOW
K XU
FCDD RLS CL
M DUBINSKIY
FCDD RLS E
RD DELROSARIO
FCDD RLS ED
K JONES
FCDD RLS EA
A ZAGHLOUL
FCDD RLS S
WL BENARD
FCDD RLS SO
W ZHOU
FCDD RLW
S KARNA
JF NEWILL
AM RAWLETT
SE SCHOENFELD
J ZABINSKI
FCDD RLW B
R BECKER
FCDD RLW M
ES CHIN
B CHEESEMAN
K CHO
FCDD RLW MB
B LOVE
D MAGAGNOSC
T WALTER
FCDD RLW MF
K DOHERTY
D FIELD
B HORNBUCKLE
K LIMMER
M WALOCK
FCDD RLW S
V CHAMPAGNE
AL WEST
FCDD RLW T
RZ FRANCART
FCDD RLW TA
M COPPINGER
FCDD RLW TC
JD CLAYTON
J LLOYD
C MEREDITH
FCDD RLW TF
J MONTGOMERY
P JANNOTTI
FCDD RLW W
TV SHEPPARD
FCDD RLW WA
B RICE
R PESCE-RODRIGUEZ
FCDD RLW M
A HALL

1 DEVCOM GVSC
(PDF) FCDD GVS IEE MAT
K SEBECK